ACS Macro Letters

Letter

pubs.acs.org/macroletters

Theory of Entanglements and Tube Confinement in Rod−Sphere Nanocomposites

Umi Yamamoto[†] and Kenneth S. Schweizer*[,‡,§]

[†]Department of Physics, [‡]Departments of Materials Science and Chemistry, and [§]Frederick Seitz Materials Research Laboratory, University of Illinois, Urbana, Illinois 61801, United States

Supporting Information

ABSTRACT: We formulate a microscopic theory for the polymer transverse confinement length and associated dynamic potential for a mixture of infinitely thin rods and hard spheres based solely on topological entanglements and excluded volume constraints. For fixed spheres, the needle effective tube diameter decreases with particle loading, and is largely controlled by a single dimensionless parameter involving all three key length-scales in the problem. A crossover from polymer entanglement to nanoparticle-controlled tube localization with increased loading is predicted. A preliminary extension to chain melts exhibits reasonable agreement with a recent simulation, and experimentally testable predictions are made. This work establishes a first-principles theoretical foundation to investigate a variety of dynamical problems in entangled polymer nanocomposites.

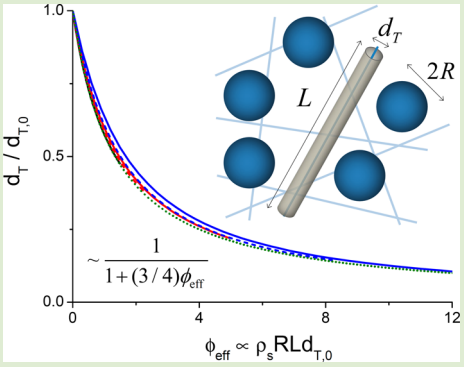

Slow dynamics of macromolecules in the presence of spherical objects is a ubiquitous problem in soft matter science. Rod-like polymers are an extensively studied class for which rich dynamical behavior occurs, for example, the anomalous transport of proteins in crowded cellular environments,[1] colloidal motion in filamentary gels,[2] and motion of stiff biopolymers in porous media.[3] Of central interest to materials science is polymer nanocomposites (PNC), where the addition of nanoparticles (NP) to macromolecular liquids can induce strong modifications of various properties.[4] Theoretical understanding of such hybrid polymer−particle systems is in its infancy.

In the absence of particles, a successful description of the entangled dynamics of polymer liquids is given by the reptation-tube model.[5] However, an extension to PNCs is difficult due to its strongly phenomenological treatment of entanglement physics. For example, the presence of multiple length-scales, internal polymer−particle interfaces, and the finite excluded volume of NPs render unclear the validity of the reptation ansatz and the nature of an effective tube. We believe the first and most fundamental question to address is how the apparent tube diameter (transverse polymer localization length), which controls elasticity and long-time dynamics in pure polymers, is modified in PNCs. This question has begun to be studied very recently via experiment and simulation.[6−9] It has been found that NPs reduce the apparent tube diameter, with a crossover from polymer entanglement to NP-controlled confinement[8] occurring at high NP loading.[7,8] No microscopic theory exists for this problem.

In this Letter, we present the first statistical-mechanical theory for the effective transverse confinement length and associated dynamic tube potential of entangled rods in a matrix of fixed hard spheres (diameter $2R$) based *solely* on topological uncrossability and the rod−sphere excluded volume constraint. Rods are modeled as infinitely thin nonrotating topological objects ("needles" of length L), the statistical microstructure is taken to be random, and the focus is on rod concentrations above the critical entanglement reduced density, $\rho_r L^3 > \rho_e L^3 \sim 10$.[10−12] Two new dimensionless length-scale ratios enter: an "aspect ratio", $L/2R$, and the NP to the "bare" (pure polymer liquid) tube diameter ratio, $d_{T,0}/2R$, which quantifies how particles fit into the entanglement mesh (see Figure 1). A preliminary extension to entangled chains based on recently developed coarse-graining and mapping ideas[13] is also briefly discussed.

Technical details of the theory development are given in the Supporting Information, and here we sketch the key physical ideas. We generalize the first-principles dynamical theory for pure topologically entangled needle liquids developed by Szamel.[10,11] This approach has successfully derived the emergence of a tube, the tube diameter, and diffusion constants[10,11] and has been recently shown to quantitatively agree with simulations of the transverse and rotational diffusion constants of needle fluids over all concentrations.[12] Our generalization of this approach requires formulating tractable coupled Smoluchowski equations for both rods and spheres in the mixture. The theory *exactly* enforces polymer−polymer topological uncrossability *and* polymer−NP impenetrability at the two-body level, and approximately captures all higher order many-body collision effects via a self-consistent renormalization

Received: September 4, 2013
Accepted: October 8, 2013
Published: October 11, 2013

   dx.doi.org/10.1021/mz4004634 | *ACS Macro Lett.* 2013, 2, 955−959

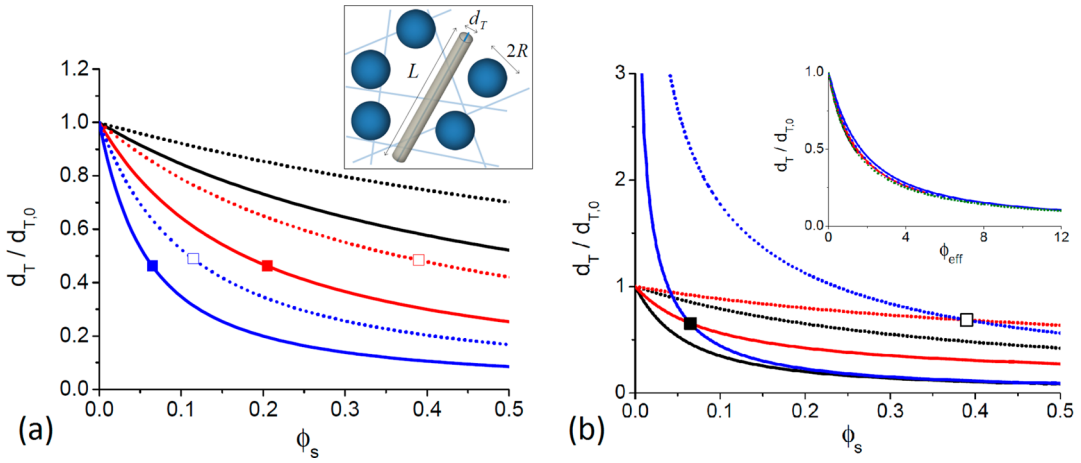

Figure 1. (a) Needle tube diameter normalized by the particle-free value as a function of sphere volume fraction. Three aspect ratios ($L/2R$ = 2, 4, and 8 from top-to-bottom) with $\rho_r L^3$ = 20 (solid) and $\rho_r L^3$ = 40 (dash) are employed. Squares indicate the crossover to the NP-confined regime defined in the text and (b). The cartoon illustrates the studied needle-sphere composite system and defines length scales. (b) Effective tube diameter and master curve. The reduced tube diameter (black) is shown for ($\rho_r L^3$, $L/2R$) = (20, 8) (solid) and (40, 4) (dot); d_{rod} (red) and d_{NP} (blue) are defined in the text. Squares indicate the crossover ϕ_S to the NP-confined regime beyond which $d_{NP} < d_{rod}$. (Inset) Replot of the figure as a function of ϕ_{eff}, with the same color code and line types. Note the good collapse and the accuracy of eq 4 (shown by green dot).

of the dynamic evolution operator. The analysis yields two coupled self-consistent equations for the frequency-dependent generalized diffusion tensors of spheres and rods. In this initial study, the theory is further simplified by adopting the fixed sphere condition, and polymer longitudinal (reptation) motion is frozen in the spirit of primitive path simulations[6,7] to compute the needle transverse localization length or tube diameter ($d_T \equiv 2r_l$) . The resulting expression is[14]

$$\frac{4}{r_l^2} = \frac{1}{2}(1 - \vec{u}_1\vec{u}_1):\sum_{\alpha=r,s}\rho_\alpha \int D\vec{r} g^{(r\alpha)}(\vec{r})\vec{T}^{(r\alpha)}(\vec{r}) \times [\Omega_{loc}^{(r\alpha)\dagger}]^{-1}\vec{T}^{(r\alpha)}(\vec{r}) \quad (1)$$

where r_l^2 is the mean-square transverse localization length, $r_l^2 \equiv \langle[r_\perp(t \to \infty) - r_\perp(0)]^2\rangle$, r and s indicate rods and spheres, $\vec{r}$ is the center-of-mass separation of two particles, $\vec{u}_i$ is the orientation vector of rod i, ρ_α is the number density of species α, $g_{r\alpha}$ are the pair correlation functions (including orientational variable where necessary), the colon represents a double contraction of tensorial indices, and $D\vec{r}$ denotes the measure of integration where $D\vec{r} = d\vec{r}d\vec{u}_2/4\pi$ if $\alpha = r$, and $D\vec{r} = d\vec{r}$ otherwise. The quantities $\Omega_{loc}^{(rr)\dagger} \equiv 1 - (r_l^2/4)(\vec{\nabla} + \vec{T}^{(rr)})\cdot(2I - \vec{u}_1\vec{u}_1 - \vec{u}_2\vec{u}_2)\cdot\vec{\nabla}$ and $\Omega_{loc}^{(rr)\dagger} \equiv 1 - (r_l^2/4)(\vec{\nabla} + \vec{T}^{(rs)})\,(I - \vec{u}_1\vec{u}_1)\cdot\vec{\nabla}$ correspond to the adjoint of the effective evolution operators that describe the long-time localized dynamics under the influence of rod−rod and rod−sphere collisions entering via the T-operator, $\vec{T}^{(r\alpha)}$.[15] Physically, eq 1 self-consistently relates the mean square tube diameter to the unrelaxed (*localized*) part of the long-time force−force time correlation function as discussed in the context of glass physics.[16−18] Here, the role of "force" is played by the T-operator that imposes the transverse dynamic uncrossability and excluded volume constraints in the form of an "impulsive" force.

Solving eq 1 involves Laplace-like partial differential equations with nontrivial boundary conditions on a curved surface. The mathematical analysis is sketched in the Supporting Information, yielding the explicit self-consistent equation for r_l:[14]

$$\left(\frac{1}{r_l}\right)^2 = K_\perp^{(rr)}(r_l) + K_\perp^{(rs)}(r_l) \quad (2)$$

$$K_\perp^{(rr)}(r_l) \equiv \frac{\pi}{8\sqrt{2}}\rho_r L\left[\frac{L}{r_l} - I_1\left(\frac{2L}{r_l}\right) + L_1\left(\frac{2L}{r_l}\right)\right] \quad (3a)$$

$$K_\perp^{(rs)}(r_l, \phi_s, \gamma) \equiv \frac{3}{2}\phi_s\left(1 + \frac{L}{2R}\right)\left(\frac{1}{2Rr_l}\right)\frac{K_0(2R/r_l)}{K_1(2R/r_l)} \quad (3b)$$

where I_n (K_n) is the modified Bessel function of first (second) kind and L_1 is the modified Struve function of first kind, and $\phi_s \equiv 4\pi R^3/3$ is the sphere volume fraction. Equation 2 determines an apparent tube diameter in terms of two physically transparent contributions associated with rod−rod and rod−sphere collisions, which are self-consistently coupled via the localization length. Fixed spheres always enhance the rod−sphere confinement effect (decrease d_T), whereas rod−rod entanglement can be either weakened or strengthened as particles are added. Specifically, in solution the spheres can occupy open spaces between rods, and thus, ρ_r can be independently controlled. In contrast, for dense melts at fixed total volume, extra space is required to insert spheres and thus ρ_r may be reduced accordingly as $\rho_r \to \rho_r(1 - \phi_s)$ ("dilution" effect). How d_T depends on the three dimensionless variables, $L/2R$, $d_{T,0}/2R$, ϕ_s reflects a subtle competition of effects.

Figure 1a shows calculations based on eq 2 for weakly and modestly entangled systems where the dilution effect is neglected. In accord with intuition, d_T decreases as ϕ_s or $L/2R$ grows, and the trend monotonically weakens at higher ρ_r due to the increasing importance of needle−needle entanglements. Remarkably, the inset of Figure 1b shows that all the results can be collapsed onto a master curve based on an effective confinement parameter, $\phi_{eff} \equiv \phi_s(d_{T,0}/2R)(1 + L/2R)$ or $\phi_{eff} \propto \rho_s R d_{T,0} L$ for $L \gg 2R$, which involves all three lengths of the system. Moreover, one can derive from eq 3 an asymptotic analytic expression for the reduced tube diameter in the $r_l \ll L$, $2R$ limit:[14]

dx.doi.org/10.1021/mz4004634 | *ACS Macro Lett.* 2013, 2, 955−959

$$\frac{d_T}{d_{T,0}} = \left[1 + \frac{3}{4}\phi_s\left(\frac{d_{T,0}}{2R}\right)\left(1 + \frac{L}{2R}\right)\right]^{-1} = \left(1 + \frac{3}{4}\phi_{eff}\right)^{-1} \quad (4)$$

This provides the physical basis for the data collapse in Figure 1b, and eq 4 agrees extremely well with the form of the master curve. Equation 4 suggests the tube reduction is controlled by the filler volume fraction and two dimensionless length-scale ratios, $d_{T,0}/2R$ and $L/2R$, or one can view $\phi_{eff} \propto \rho_s R d_{T,0} L$ as the single key quantity that determines how NPs modify rod transverse localization. Specifically, it has the following physical and geometric interpretation; $\rho_s R d_{T,0} L$ is proportional to the average number of NPs that penetrate into the cylindrical region of space defined by the bare tube (diameter $d_{T,0}$) while maintaining the excluded volume constraint with the tagged rod.[14]

Another fundamental question is how much of the tube localization originates from rod−rod forces or collisions compared to the rod−sphere analog. A phenomenological analysis has been proposed for chain melts based on the additive ansatz, $1/d_{app}^2 = 1/d_{tube}^2 + 1/d_{geo}^2$, where d_{app} is the "apparent" tube diameter determined from neutron spin echo experiments, d_{geo} is the mean geometric distance between a polymer segment and a NP, and d_{tube} is the polymer−polymer entanglement length deduced (defined) from the two other quantities.[8] Our theory can microscopically address this issue by identifying $1/d_{rod}^2$ ($1/d_{NP}^2$) with the first (second) term of eq 2. At large ϕ_s, Figure 1b shows d_{NP} becomes smaller than d_{rod}, demonstrating a crossover to the "NP confinement" regime.[7,8] This crossover disappears at large (small) enough values of $\rho_r L^3$ ($L/2R$) where inter-rod entanglements dominate tube localization. We emphasize that our d_{NP} is a consequence of many-body collisions and dynamic localization and, hence, is not identical to d_{geo}.

The full dynamic tube confinement potential for transverse rod motion in nanocomposites can be constructed based on the well-established nonlinear Langevin equation (NLE) approach.[17,18] The pure-needle application of NLE theory has been shown to quantitatively agree[12] with experimental measurements[19] of the non-Gaussian tube confinement potential in heavily entangled f-actin solutions. NLE theory is based on a stochastic evolution equation for transverse needle displacement, $-\zeta_s(dr_\perp/dt) - (\partial/\partial r_\perp)F_{dyn}(r_\perp) + \delta f_s = 0$, where ζ_s is the short-time friction coefficient, δf_s is the corresponding random fluctuating force, and $F_{dyn}(r_\perp) = -\int_{r_l}^{r_\perp} f(r)dr$ is the dynamic confinement potential obtained via integrating the transverse caging force:

$$f(r_\perp) = \frac{2k_BT}{r_\perp} - 2k_BT[r_\perp K_\perp^{(rr)}(r_\perp) + r_\perp K_\perp^{(rs)}(r_\perp)] \quad (5)$$

By construction of the NLE approach, setting eq 5 to zero and solving for $r_\perp$ yields eq 2, that is, the position of mechanical equilibrium of $F_{dyn}(r_\perp)$ agrees with $r_l = d_T/2$ obtained above.

Figure 2 presents calculations of the normalized transverse displacement distribution, $P(r_\perp) \propto e^{-\beta F_{dyn}(r_\perp)}$. One sees that adding NPs monotonically tightens the distribution, while the anharmonic shape and exponential tail previously predicted for pure needle fluids[12] remain present. Interestingly, the shape of F_{dyn} is nearly (but not exactly) universal if the relative displacement is scaled by r_l,[12] implying that the effect of NPs on the anharmonic transverse displacement distribution is, to leading order, captured by simply renormalizing the tube

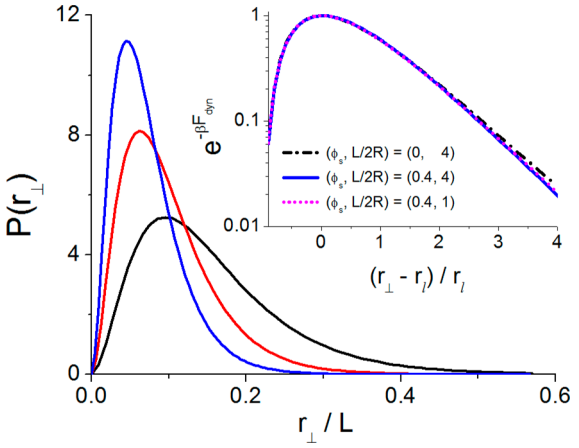

Figure 2. Transverse displacement distributions for needles. Results are shown for $\rho_r L^3 = 40$, $L/2R = 4$, and $\phi_s = 0$, 0.2, and 0.4 (from right to left). (Inset) Un-normalized distribution as a function of transverse displacement relative to the minimum of F_{dyn} and reduced by r_l for $\rho_r L^3 = 40$ and the displayed values of (ϕ_s, $L/2R$).

diameter. The latter simplification is further supported by the following two findings: to an excellent approximation, $\langle r_\perp \rangle \propto d_T/2$, and the maximum confining force, f_{max}, obeys the same relation as for a pure needle fluid, $f_{max} \sim 2k_BT(r_l^{-1} - r_m^{-1})$, where the location of the maximum is $r_m \sim L/[4L/(\pi d_{T,0}) + (3/4)\phi_s(L/2R)^2(1 + L/2R)]^{1/2} \sim (2r_lL)^{1/2}$ when eq 4 applies.

Extending our theory to flexible chain melt nanocomposites is a challenging task. Even for pure polymers at a primitive path (PP) level of description, development of a microscopic theory is difficult due to a large number of correlated collisions between a pair of interpenetrating and uncrossable coils.[13] The technical challenges significantly grow in PNCs, and one expects distinct physical regimes including (i) small NPs ($2R \ll d_T$) akin to solvents that dilute the entanglement network, (ii) large ($2R \gg d_T$ or R_g) effectively immobile NPs, which simultaneously confine multiple primitive paths,[5] and (iii) intermediate-size ($2R \sim d_T$) NPs that may affect the confinement tube only on the "local" scale of a single PP.

As a first theoretical attempt, we consider two approximate approaches for regimes (ii) and (iii) motivated by recent coarse-graining and mapping ideas successfully developed for entangled chain liquids.[13] The first represents a coil by a freely jointed chain of PP steps of length L_e, which is determined self-consistently and microscopically. For treating tube localization, this mapping can be viewed as a fluid of disconnected primitive path (dPP) segments modeled as uncrossable needles of $L_e = 5r_l$.[13] The reduced rod density $\rho_r L^3$ then maps to L_e/p, where p is the invariant packing length[20] that may be fixed independently or varies with ϕ_s to reflect the dilution effect. The second "super-coarse-graining" (SCG) method maps an entire chain to a single end-to-end vector needle via $L \to R_{ee}/(1.3)^{1/2}$ based on the instantaneous polymer conformational anisotropy and implies $\rho_r L^3 \to 10.54(N/N_e)^{1/2}$.[13] Both approaches, in combination with the entangled needle theory,[12] agree well[13] with experiments[20] and simulations[21] for the tube diameter scaling with packing length and the full PP distribution in entangled chain melts. For PNCs, the usefulness of these coarse-graining approaches is a priori unknown and likely depend on the length-scale ratios of interest. Physically, the dPP model seems most reasonable when $2R < d_T$, while the SCG mapping seems more appropriate if $2R > R_{ee}$; the latter

dx.doi.org/10.1021/mz4004634 | ACS Macro Lett. 2013, 2, 955−959

condition is equivalent to $2R/d_{T,0} > (N/N_e)^{1/2}$ based on $d_{T,0} = N_e^{1/2}\sigma$.

The above ideas are first tested against the entangled melt simulation of ref 7 where $d_{T,0}/2R \approx 1.2$, $N/N_e \approx 10$ and $R_{ee}/2R \approx 2.8$. We set $p(\phi_s) = p(0)/(1 - \phi_s)$ to reflect the change of polymer number density in the simulation; $d_{polymer}$ and d_{NP} are obtained in analogy to the needle-sphere theory described above. Figure 3 shows the predicted tube diameter reduction

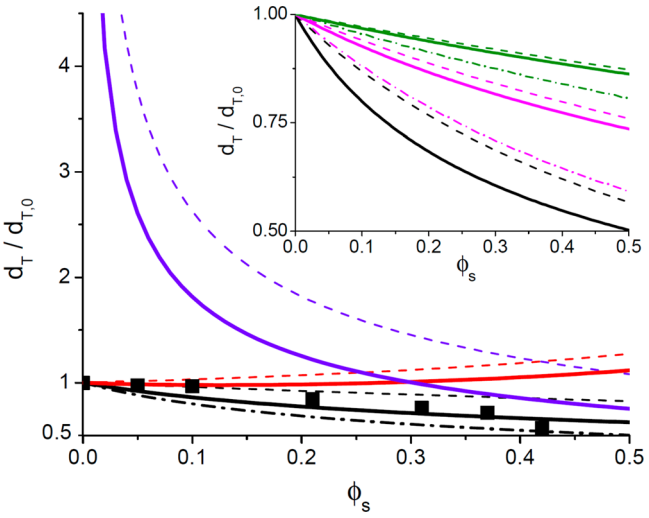

Figure 3. Reduced tube diameter as a function of sphere volume fraction for flexible chain melts. Predictions are made using the dPP (solid and dash dot) and SCG (dash) models. Black, red, and blue curves are the apparent tube diameter, $d_{polymer}$, d_{NP}, respectively, while squares are the simulation result[7] for the apparent tube diameter. The dash-dot curve is the dPP result without the dilution effect. (Inset) Predictions without the dilution effect based on SCG (solid) and dPP (dot). Colors correspond to three representative systems motivated by recent experiments where $(2R/d_{T,0}, 2R/R_{ee}, N/N_e) \approx (3.4, 0.84, 17)$[8] (green), (1.9, 0.64, 8.2)[22] (pink), and (0.83, 0.36, 10)[7] (black). Dash-dot curves represent the SCG mapping result with $N/N_e = 100$ and the same values for $(2R, d_{T,0})$.

with NP loading is in good agreement with simulation, and the two key features are captured: (i) the location of the crossover to the NP-confined regime, and (ii) the reduced interpolymer entanglement confinement with increasing NP volume fraction. Note that our $d_{polymer}$ is extracted in the presence of (and is coupled to) the NPs, different from how d_{tube} was obtained in ref 7 via the "phantom particle" model.[6,7] Nevertheless, we do find an upturn of $d_{polymer}$ corresponding to an effective reduction of polymer−polymer entanglement, which is mainly due to the increasing packing length with NP addition. Removing this dilution effect reverses the trend of $d_{polymer}$, but the effective tube diameter is only weakly modified. On the other hand, the SCG model exhibits larger deviations from simulation, as expected according to the physical length-scale criteria discussed above.

Additional calculations without the dilution effect are shown in the inset of Figure 3 for parameters associated with recent experimental studies that involve silica NPs dissolved in melts of PEP[8] or PMMA.[22] Both dPP and SCG results are shown since these systems do not cleanly fall into the $2R/R_{ee} > 1$ or $2R < d_T$ regimes. One sees that both theoretical models underestimate the silica-PEP data of ref 8, where d_T drops by 30% at $\phi_s = 0.6$. Increasing N/N_e in the SCG model results in the qualitatively new prediction that longer chains exhibit greater tube reduction due to polymer connectivity effects, and a similar trend is predicted upon decreasing the NP diameter (not shown). Given the current theoretical simplifications, our results for these flexible chain nanocomposites require future testing via carefully designed experiments or simulations.

In summary, we have constructed a first-principles theory for tube localization of a fluid of topologically entangled needles dissolved in a matrix of fixed hard spheres. This work provides a foundation for developing new theories for a variety of open problems, such as (i) anisotropic needle diffusion in immobile obstacle matrices, (ii) the role of filler mobility on tube confinement and transport, (iii) inclusion of nonrandom packing effects and intermolecular attractions (composite microstructure) on entangled polymer and filler dynamics, and (iv) a more rigorous treatment of flexible chain nanocomposites. Work is in progress in all these directions.

■ ASSOCIATED CONTENT

Supporting Information

The most essential steps to derive eqs 1−4. This material is available free of charge via the Internet at http://pubs.acs.org.

■ AUTHOR INFORMATION

Corresponding Author

*E-mail: kschweiz@illinois.edu.

Notes

The authors declare no competing financial interest.

■ ACKNOWLEDGMENTS

We thank Ying Li and Martin Kröger for sending their simulation data. This research was supported by Michelin-France.

■ REFERENCES

(1) Banks, D. S.; Fradin, C. *Biophys. J.* **2005**, *89*, 2960−2971.
(2) Wong, I. Y.; Gardel, M. L.; Reichman, D. R.; Weeks, E. R.; Valentine, M. T.; Bausch, A. R.; Weitz, D. A. *Phys. Rev. Lett.* **2004**, *92*, 178101.
(3) Golding, I.; Cox, E. C. *Phys. Rev. Lett.* **2006**, *96*, 098102.
(4) Balazs, A. C.; Emrick, T.; Russel, T. P. *Science* **2006**, *314*, 1107−1110.
(5) Doi, M.; Edwards, S. F. *The Theory of Polymer Dynamics*; Clarendon Press: Oxford, 1986.
(6) Toepperwein, G. N.; Karayiannis, N. C.; Riggleman, R. A.; Kröger, M.; de Pablo, J. J. *Macromolecules* **2011**, *44*, 1034−1045.
(7) Li, Y.; Kröger, M.; Liu, W. K. *Phys. Rev. Lett.* **2012**, *109*, 118001.
(8) Schneider, G. J.; Nusser, K.; Willner, L.; Falus, P.; Richter, D. *Macromolecules* **2011**, *44*, 5857−5860.
(9) Karatrantos, A.; Clarke, N.; Composto, R. J.; Winey, K. I. *Soft Matter* **2013**, *9*, 3877−3884.
(10) Szamel, G. *Phys. Rev. Lett.* **1993**, *70*, 3744−3747.
(11) Szamel, G.; Schweizer, K. S. *J. Chem. Phys.* **1994**, *100*, 3127−3141.
(12) Sussman, D. M.; Schweizer, K. S. *Phys. Rev. Lett.* **2011**, *107*, 078102.
(13) Sussman, D. M.; Schweizer, K. S. *Phys. Rev. Lett.* **2012**, *109*, 168306.
(14) See Supporting Information.
(15) Cichocki, B. *Z. Phys. B* **1987**, *66*, 537−540.
(16) Hansen, J. P.; McDonald, I. R. *Theory of Simple Liquids*; Academic Press: London, 1986.
(17) Schweizer, K. S.; Saltzman, E. J. *J. Chem. Phys.* **2003**, *119*, 1181−1196.
(18) Schweizer, K. S. *J. Chem. Phys.* **2005**, *123*, 244501.

(19) Wang, B.; Guan, J.; Anthony, S. M.; Bae, S. C.; Schweizer, K. S.; Granick, S. *Phys. Rev. Lett.* **2010**, *104*, 118301.
(20) Fetters, L. J.; Lohse, D. J.; Richter, D.; Witten, T. A.; Zirkel, A. *Macromolecules* **1994**, *27*, 4639−4647.
(21) Tzoumanekas, C.; Theodorou, D. N. *Macromolecules* **2006**, *39*, 4592−4604.
(22) Lin, C.; Gam, S.; Meth, J. S; Clarke, N.; Winey, K. I.; Composto, R. J. *Macromolecules* **2013**, *46*, 4502−4509.